

Doping-dependent band structure of $\text{LaAlO}_3/\text{SrTiO}_3$ interfaces by soft x-ray polarization-controlled resonant angle-resolved photoemission

C. Cancellieri,* M. L. Reinle-Schmitt, M. Kobayashi, V. N. Strocov, and P. R. Willmott

Swiss Light Source, Paul Scherrer Institut, CH-5232 Villigen, Switzerland

D. Fontaine and Ph. Ghosez

Physique Théorique des Matériaux, Université de Liège,

Allée du 6 Août 17 (B5), 4000 Sart Tilman, Belgium

A. Filippetti, P. Delugas, and V. Fiorentini

CNR-IOM UOS Cagliari, Dipartimento di Fisica, Università di Cagliari,

SP Monserrato-Sestu km.0.700, 09042 Monserrato (CA), Italy

(Dated: August 14, 2018)

Abstract

Polarization-controlled synchrotron radiation was used to map the electronic structure of buried conducting interfaces of $\text{LaAlO}_3/\text{SrTiO}_3$ in a resonant angle-resolved photoemission experiment. A strong dependence on the light polarization of the Fermi surface and band dispersions is demonstrated, highlighting the distinct Ti $3d$ orbitals involved in 2D conduction. Samples with different 2D doping levels were prepared and measured by photoemission, revealing different band occupancies and Fermi surface shapes. A direct comparison between the photoemission measurements and advanced first-principle calculations carried out for different $3d$ -band fillings is presented in conjunction with the 2D carrier concentration obtained from transport measurements.

PACS numbers: 79.60.Jv, 73.20.-r, 31.15.A-

Complex-oxide interfaces exhibit a broad spectrum of electronic properties and complex phase diagrams and have thus attracted considerable attention. A particularly interesting example is the appearance of 2-dimensional (2D) conductivity at the interface between the band insulators LaAlO_3 (LAO) and SrTiO_3 (STO) [1–3] above a critical LAO thickness of 3 unit cells (u.c.) [4]. As revealed by *ab-initio* calculations [5, 6], the mobile electron charge of this 2-dimensional system (2DES) is confined in conduction bands of $3d\ t_{2g}$ orbital character extending over a few STO layers from the interface and is thus very different from that of doped STO bulk. However, the detailed characteristics of these conduction bands crucially depend on the amount of carriers present at the interface. It follows that a comparison between observed and calculated electronic properties of the interface only makes sense if referred to the same carrier concentration.

The band structure calculated for 0.5 electrons per u.c. ($3.5 \times 10^{14} \text{ e/cm}^2$), that is the value needed to suppress the “polar catastrophe” due to the diverging potential in polar LAO [7], is often taken as “reference”. In fact, the experimentally determined mobile carrier density in LAO/STO is always much smaller than that. Typical experimental values reported for the 2D-carrier density, n_s , measured by Hall effect at 100 K are between 10^{13} and 10^{14} e/cm^2 [8]. This suggests an important partial charge localization or other charge-compensating mechanisms such as surface passivation or reconstruction [9, 10].

Direct access to the electronic band structure is a crucial step towards the full understanding of complex-oxide interfaces. Angle-resolved photoemission spectroscopy (ARPES) is a powerful technique which yields a map of photoelectron intensities as a function of their kinetic energies and momentum, revealing the electronic structure in solids. Recent ARPES studies on bare STO surfaces [11–13] have shown the formation of a 2DES which appears to have similar properties to those of the LAO/STO interfacial conducting layer. Photoemission spectroscopy of buried interfaces is more challenging due to the small inelastic electron mean free path in solids, which, over a wide range of photon energies ($h\nu$), is of the order of 1 nm. However, it was shown recently that a combination of soft x-ray photoemission with resonant photoexcitation [14–18] can overcome this limitation. By selecting $h\nu$ at the Ti L edge, the signal of the Fermi states associated with conducting electrons is greatly enhanced in LAO/STO interfaces. Berner and coworkers [18] were the first to report on the Fermi surface (FS) of the LAO/STO interface, confirming the strong similarities between bare STO and STO-based heterostructures. Here we report the first photoemission measure-

ments resolved in both angle and photon polarization which are thus capable to distinguish different orbital contributions to the bands and FSs.

We have correlated the FS shape with the number of carriers measured by magneto-transport, investigating samples with different n_s . The FS and band dispersions visible in the photoemission experiment are highly dependent on the incident photon light polarizations and on n_s , suggesting a strong orbital character and different band filling of these heterostructures. The experimental data are complemented by *ab-initio* results which for the first time describe the detailed evolution of band energies and FS with the charge density present at the interface, in a density range ($\sim 10^{13}$ e/cm²) consistent with that measured for the investigated samples. This provides an unprecedented, direct comparison of calculated and measured electronic properties at equal doping. Our photoemission band dispersions and theoretical calculations coherently reproduce the orbital decomposition of charges at the given transport-derived carrier density, thus clarifying the exact 3d level electron occupancy in this system. The possible contribution of photocarriers induced by x-ray radiation was investigated and only an insignificant effect on the electronic structure was measured. Details are given in the Supplementary Materials.

LAO thin films were grown by pulsed laser deposition on (001)-oriented TiO₂-terminated STO substrates at 800 °C in an oxygen pressure of 8×10^{-5} mbar. These “standard” LAO/STO samples have transport properties similar to those reported in Ref. 8, with $n_s \sim 4 - 6 \times 10^{13}$ e/cm², measured by the Hall effect (SD samples). Samples with lower 2D-carriers densities (LD samples) have been also prepared using a growth temperature of 650 °C, as reported in Ref. 19. These latter samples have a $n_s \sim 10^{13}$ e/cm². A KrF excimer laser (248 nm) was used to ablate the sintered targets with a fluence of 0.6 J/cm² at a frequency of 1 Hz, leading to a deposition rate of about one unit cell for ~ 60 pulses. After deposition, the oxygen pressure was raised to 0.2 bar and the temperature maintained at 540 ± 10 °C for one hour, in order to ensure full oxidation [20]. Film growth was monitored *in-situ* by reflection high-energy electron-diffraction. The critical thickness required to undergo an insulator-to-metal transition was 4 u.c., as reported in Ref. 4. Our conducting interfaces had a LAO thickness between 4 and 5 u.c.

For *ab-initio* calculations we used an advanced variant of density functional theory, i.e., the variational pseudo self-interaction correction (VPSIC) [21] capable of correcting the imperfect description of standard local-density functionals and reproduce the band-gap of

oxide-based systems and the band alignment at the LAO/STO interface [6]. The different carrier density regimes are described starting from the insulating interface (i.e. for LAO thickness smaller than 4 u.c.) and, while keeping the LAO thickness fixed, introducing an increased amount of electron charge in the system, and leaving the system to fully relax to its structural and electronic ground state (in practice mimicking a field-effect-induced charge accumulation). In this way we can monitor the evolution of the electronic properties due to very tiny and well defined changes of electron charge, comparable in magnitude with the Hall-measured values.

The measurements were performed at the soft-x-ray ARPES endstation of the Advanced Resonant Spectroscopies (ADRESS) beamline [22] at the Swiss Light Source. The samples were transferred from the deposition chamber *ex-situ* without further annealing in vacuum. The beamline delivers a high photon flux, exceeding 10^{13} photons/sec/0.01% bandwidth providing excellent statistics of the interface signal, despite its attenuation as the photoelectrons pass through the film layer. Measurements were performed using different light polarizations, switching between *c*-polarized (circular), *p*-polarized (linear vertical), and *s*-polarized (linear horizontal), to excite states of different symmetries relative to the mirror plane. The experimental geometry is shown in Fig. 1(a). The measurement plane (MP) coincides with the (010) mirror plane formed by the sample normal along the [001] and the Γ -X directions. The experiment was performed at ~ 11 K. The combined beamline and analyzer energy resolution was set to around 80 meV for the valence-band spectra.

Following Ref. 17, $h\nu$ was selected at the Ti *L* absorption edge (see Supplementary Materials). We maximized the intensity at the Fermi level (E_F) at sufficient energy separation from the Ti $2p_{3/2}$ core level second order contribution and selected $h\nu$ equal to 460.3 eV. We emphasize that no presence of in-gap states could be found in the samples at any $h\nu$ (see Supplementary Materials also for results on the related $\text{La}_{0.5}\text{Sr}_{0.5}\text{Al}_{0.5}\text{Ti}_{0.5}\text{O}_3/\text{STO}$ heterostructure [23]). These in-gap states, measured in bare STO [11, 13] and very recently also in the LAO/STO interface [18, 24], appear at ~ 1 eV below the Fermi edge, are resonant with Ti^{3+} valence states, and are mainly due to surface-defects and impurity states related to oxygen vacancies [25]. These incoherent states are highly photosensitive, displaying an important photodoping effect. Our oxygen-annealed samples show no such contributions from the oxygen vacancies to the 2D electrical conduction, confirmed by the absence of photodoping. The ARPES data obtained with *c*-polarized photons for a standard LAO/STO sample

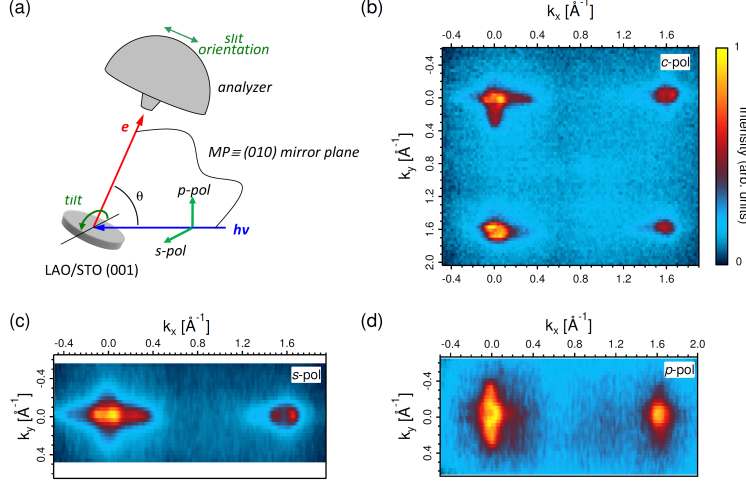


FIG. 1. (Color online)(a) Experimental geometry setup for polarization dependent measurements; the tilt and θ angles allow the in-plane k -space mapping. (b) FS maps collected for 4 Brillouin zones with circular polarized light at $h\nu = 460.3$ eV; FS maps using (c) s -polarized and (d) p -polarized radiation. The data shown are for a SD sample.

shown in Fig. 1(b) reveal non-equivalent shapes of the FS in different Brillouin zones, in agreement with Ref. 18. This behavior can be ascribed to different matrix elements acting on the photoemission intensity from different interface bands, revealing the compound character of the LAO/STO interface states. The linear dichroism of the spectra, shown in Figs. 1(c) and (d), show more clearly and in detail the multiple-state character of these electronic FS components, which are strongly polarization-dependent. The different photon-polarization measurements reveal that the FS is made up of a circle, originating mainly from Ti $3d_{xy}$ bands, and two ellipsoids aligned along the k_x and k_y directions, due to the heavy d_{yz} and d_{xz} band contributions. A comparison between the p - and s -polarized data in Fig. 1 agrees with the $3d$ orbital character of the FS. The intensity of each band is modulated by the matrix element (photon excitation probability) which depends on the symmetry of the band, the polarization of the incident photons, and their relative angle.

By switching the incident light polarization from p - to s -polarization, states symmetric and antisymmetric, respectively, with respect to a (010) MP mirror reflection are excited, thereby selecting the different symmetries of the valence states. Thus, with s -polarization, only the d_{xy} and d_{yz} states of odd symmetry relative to the MP are detected, while, for p -polarized light, only d_{xz} bands with even symmetry with respect to the mirror plane are

observed. In Fig. 1(c) (*s*-polarization) the cigar-shaped d_{yz} FS is clearly visible, stretched along the k_x axis, and superimposed on the circular-shaped d_{xy} FS. In Fig. 1(d) (*p*-polarized) only d_{xz} is visible, recognizable by the long side stretched along k_y .

Fig. 2(a)-(f) and Fig. 3(a)-(f) show *s*-polarized and *p*-polarized photoemission data respectively, collected around the Γ point along the Γ -X- Γ' direction, for both SD and LD samples. Measurements on a LD sample results in a different band dispersion and FS as shown in Fig. 3(b): the d_{xz} orbitals are almost no longer visible, highlighting the effect of the doping level on the filling of the bands. The different dispersion signals in the intensity plot Figs. 2(a), 3(c) and (e), and shown more clearly in the negative second derivative plots of Figs. 2(b), 3(d) and (f), demonstrate that different bands are enhanced or suppressed by the polarization geometry.

In Fig. 2 are presented the photoemission data acquired with *s*-polarized light. The experimental broadening of the signal at this $h\nu$ precludes the possibility of resolving each individual Ti $3d$ band contributing to the measured photoemission. However, from the photoemission intensity maps, the second derivative plots and the energy-distribution curves (EDCs) in Fig. 2, two types of bands, one lighter and one heavier (the latter having lower intensity, thus not visible in the second Brillouin zones), can be clearly distinguished. Comparison with the VPSIC-calculated symmetries of the t_{2g} bands, superimposed on the photoemission data in Fig. 2(b) and (e), aids recognition of the orbital character of these bands. For the SD sample [Fig. 2(a)] we consider calculation for $n_s=6.5\times 10^{13}$ e/cm², at this density most of the charge is included in three bands. The lowest two bands have planar d_{xy} orbital characters, effective masses $m^* \sim 0.7$ along k_x and Fermi vectors $k_F = 0.13 \text{ \AA}^{-1}$ and 0.09 \AA^{-1} . They collect the electron charge entirely confined within the first and the second TiO₂ layer from the interface (see the Supplementary Material for the detailed analysis). The third occupied band has d_{yz} orbital character and includes charges spreading orthogonally to the interface. It is rather flat along k_x ($m^* \sim 9$ and $k_F = 0.23 \text{ \AA}^{-1}$ according to the calculations) and shifted upward in energy by about 70 meV with respect to the most occupied d_{xy} state.

In Fig. 2(e) (LD sample), we superimposed the photoemission intensity maps with bands calculated for $n_s=2.6\times 10^{13}$ e/cm². Now, d_{yz} is above E_F and empty, thus all the charge is included in the two d_{xy} bands, enclosed in circular Fermi pockets of radius $k_F=0.1 \text{ \AA}^{-1}$ and 0.06 \AA^{-1} . In agreement with the band calculations, the photoemission signal is incompatible

with the d_{yz} band.

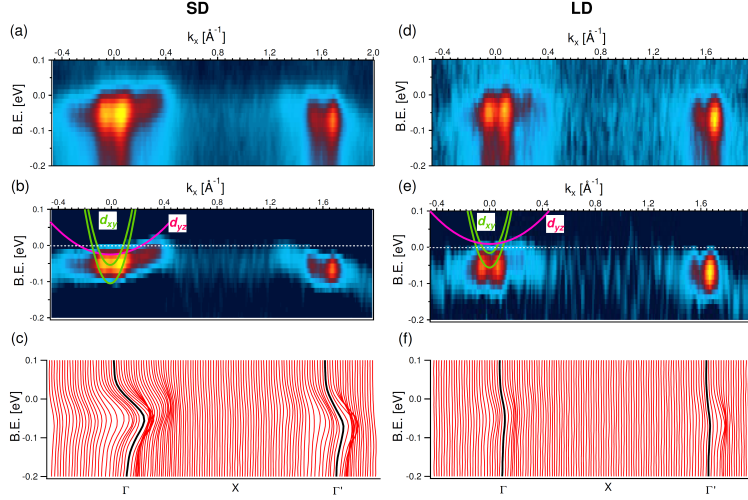


FIG. 2. (Color online) (a) ARPES data along the Γ -X- Γ' direction with s -polarized light and $h\nu = 460.3$ eV collected for a SD sample; (b) Second derivative intensity plot of data in panel (a) illustrates more clearly the band dispersion; (c) EDCs of the data in panel (a). (d)-(f) The equivalent measurements as shown in panels (a), (b) and (c) respectively, but for the LD sample. In panels (b) and (e) the calculated t_{2g} parabolic bands are shown. The color scale is the same as that shown in Fig. 1(b).

The p -polarization results are shown in Fig. 3. By symmetry, only the d_{xz} band are expected to appear, thus here we superimpose only the calculated d_{xz} band [magenta curve in Fig. 3(d) and (f)]. Due to tetragonal symmetry, the d_{xz} band bottom is degenerate with d_{yz} , and its effective mass along k_y is equal to that of d_{yz} along k_x . Thus, for the SD sample, photoemission displays a rather flat band enclosed in a cigar-shaped Fermi pocket of length $k_y \sim 0.3 \text{ \AA}^{-1}$, in good agreement with the value 0.23 \AA^{-1} calculated for $n_s = 6.5 \times 10^{13} \text{ e/cm}^2$. On the other hand, assuming again $n_s = 2.6 \times 10^{13} \text{ e/cm}^2$ for the analysis of the LD sample, the calculated d_{xz} band is completely above E_F . Some d_{xy} admixture shows up in the experiment because of finite acceptance of the analyzer, in the vicinity of the mirror plane.

The interpretation of these results can be understood from the band energies' theoretical evolution as a function of carrier density. First, it is important to realize that, while the in-plane effective masses of the t_{2g} bands are scarcely affected by the interface, their band bottom alignment with respect to E_F , as well as their mutual band splitting, are crucially dependent on the overall amount of mobile charge in the system, as clearly shown in Fig. 4

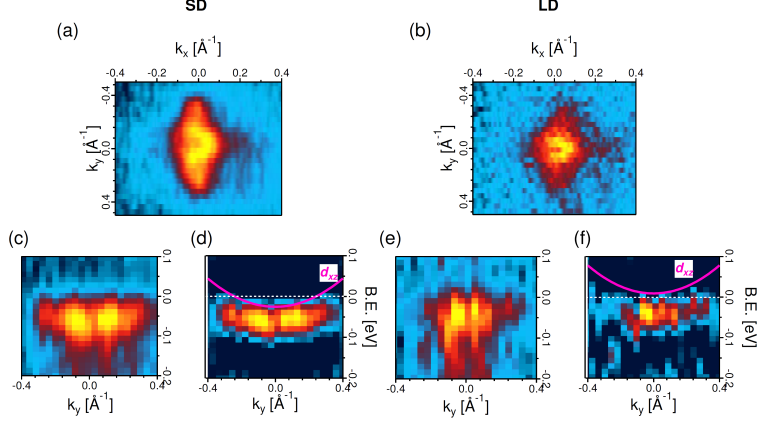


FIG. 3. (Color online) FS collected with p -polarized light and $h\nu = 460.3$ eV for (a) a SD and for (b) a LD sample. (c) ARPES data along the Γ -X direction with p -polarized light collected for a SD sample; (d) second derivative intensity plot of data in panel (c) illustrates more clearly the band dispersion; (e) and (f) the equivalent measurements as shown in panels (c) and (d) respectively, but for the LD sample. In panels (d) and (f) the calculated t_{2g} bands are superimposed. The color scale is the same as that given in Fig. 1(b).

(a detailed description is presented in the Supplementary Materials). Thus, two samples with substantially different doping may present different charge redistribution in individual orbitals, and in turn radically different photoemission response. At very low density, mobile charge accumulates in the d_{xy} bands closer to the interface [the two d_{xy} bottom energies in Fig. 4 clearly correspond to the green bands shown in Figs. 2(b) and (e)], while orthogonal d_{yz} and d_{xz} orbitals [magenta lines in Figs. 2(b), (e) and 3 (d), (f)] are initially empty. Such a d_{xy} -(d_{yz}, d_{xz}) on-site splitting is a well known consequence of the conduction band misalignment and the suppression of the interface orthogonal hopping. For increasing charge, all bands progressively shift downward in energy across E_F , until, above a certain charge threshold $n_s \sim 3.5 \times 10^{13}$ e/cm² (see Fig. 4), a portion of the charge starts to fill the orthogonal (cigar-shaped) orbitals as well. Given the different character of planar and orthogonal orbitals, crossing this threshold represents a dramatic change in optical and transport properties of the 2DES. Our photoemission data for two samples purposely prepared for having doping concentration lower and higher than the theoretically predicted threshold, demonstrates explicitly this regime change. The band bottom energies continue to evolve strongly at increasing carrier concentrations: at $n_s = 3.3 \times 10^{14}$ e/cm² corresponding to the half-electron

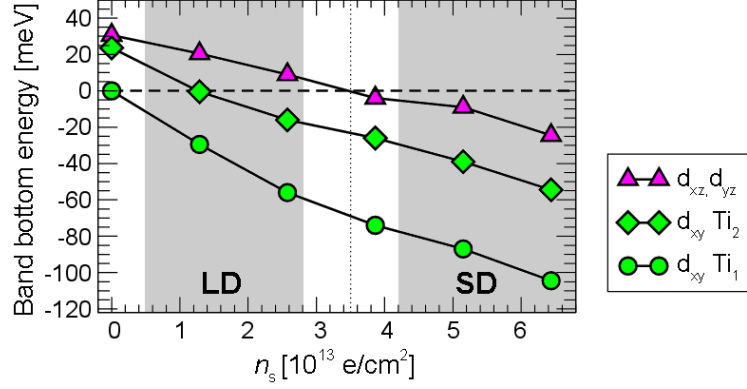


FIG. 4. (Color online) Band bottom energies with respect to $E_F=0$, as a function of the 2D carrier concentration n_s for the most important t_{2g} conduction bands, calculated by VPSIC. First and second lowest interface-parallel d_{xy} bands reside in the first and second TiO_2 layer from the interface, respectively. The dotted vertical line indicates the threshold density above which the interface-orthogonal (d_{xz} , d_{yz}) states start to contribute to photoemission and transport. Blue shaded areas span the Hall-estimated range of charge density values for LD and SD samples.

per interface u.c., the d_{xy} (Ti_1), d_{xy} (Ti_2) and d_{xz} band bottoms are located at -370, -210 and -100 meV, respectively [6]. These values are clearly incompatible with the experimental observations, demonstrating that the ideal limit dictated by the polarization catastrophe is not achieved in actual samples. These results differ from the ARPES measurements on bare STO - in contrast to the universal 2D FS of bare STO, whose size and shape are decoupled from the bulk sample preparation, it appears that the deposition of LAO with different growth conditions affects the LAO/STO 2D FS size. Moreover our dispersion curves and FSs show that the carriers involved in conductivity have a coherent character and the incoherent part (i.e. in-gap states) is negligible.

In conclusion, we have carried out a polarization-dependent ARPES experiment investigating the symmetry of the valence states and band structure of LAO/STO interfaces. We identify clearly d_{xy} , d_{yz} and d_{xz} bands and directly compare these with *ab-initio* calculations performed for different band symmetries. Two types of samples have been considered, one having a standard, the other a lower charge density. From first-principles calculations, we have shown that the position of the 3d levels is strongly dependent on the band occupancy. For both samples, ARPES spectra are compatible with the electronic band structures calculated for doping concentrations fixed to the values obtained from Hall measurements, but

not with the band structure calculated at the ideal limit of 0.5 e/u.c. expected in the polar catastrophe scenario. This demonstrates that Hall measurements properly probe the occupancy of the delocalized $3d$ levels at the interface. This work thus provides benchmark results linking the evolution of the band structure to the sheet carrier density.

The authors are grateful to J.-M. Triscone, S. Gariglio, D. Stornaiuolo and A. Fête for discussion and help in sample preparation. Support of this work by the Schweizerischer Nationalfonds zur Förderung der wissenschaftlichen Forschung, in particular the National Center of Competence in Research, Materials with Novel Electronic Properties, MaNEP. The staff of the Swiss Light Source is gratefully acknowledged. CNR-IOM scientists acknowledge MIUR-PRIN 2010 *Oxide*, IIT-Seed NEWDFESCM, IIT-SEED POLYPHEMO and “platform computation” of IIT, and Fondazione Banco di Sardegna grants. PhG acknowledges a Research Professorship of the Francqui Foundation and partial financial support from the ARC project TheMoTherm.

* claudia.cancellieri@psi.ch

- [1] A. Ohtomo and H. Y. Hwang, *Nature* **427**, 423 (2004).
- [2] N. Reyren, S. Thiel, A. D. Caviglia, L. F. Kourkoutis, G. Hammerl, C. Richter, C. W. Schneider, T. Kopp, A.-S. Rüetschi, D. Jaccard, M. Gabay, D. A. Muller, J.-M. Triscone, and J. Mannhart, *Science* **317**, 1196 (2007).
- [3] A. D. Caviglia, N. Gariglio, S. Reyren, D. Jaccard, T. Schneider, M. Gabay, S. Thiel, G. Hammerl, J. Mannhart, and J.-M. Triscone, *Nature* **456**, 624 (2008).
- [4] S. Thiel, G. Hammerl, A. Schmehl, C. W. Schneider, and J. Mannhart, *Science* **313**, 1942 (2006).
- [5] Z. S. Popovic, S. Satpathy, and R. M. Martin, *Phys. Rev. Lett.* **101**, 256801 (2008).
- [6] P. Delugas, A. Filippetti, V. Fiorentini, D. I. Bilc, D. Fontaine, and P. Ghosez, *Phys. Rev. Lett.* **106**, 166807 (2011).
- [7] N. Nakagawa, H. Y. Hwang, and D. A. Muller, *Nat. Mater.* **5**, 204 (2006).
- [8] S. Gariglio, N. Reyren, A. D. Caviglia, and J.-M. Triscone, *J. Phys. Condens. Matter* **21**, 164213 (2009).
- [9] Y. Xie, Y. Hikita, C. Bell, and H. Y. Hwang, *Nat. Commun.* **2**, 494 (2011).

- [10] N. C. Bristowe, P. B. Littlewood, and E. Artacho, *Phys. Rev. B* **83**, 205405 (2011).
- [11] W. Meevasana, P. D. C. King, R. H. He, S.-K. Mo, M. Hashimoto, A. Tamai, P. Songsiriritthigul, F. Baumberger, and Z.-X. Shen, *Nature mat.* **10**, 114 (2011).
- [12] A. F. Santander-Syro, O. Copie, T. Kondo, F. Fortuna, S. Pailhes, R. Weht, X. G. Qiu, F. Bertran, A. Nicolaou, A. Taleb-Ibrahimi, P. Le Fevre, G. Herranz, M. Bibes, N. Reyren, Y. Apertet, P. Lecoeur, A. Barthelemy, and M. J. Rozenberg, *Nature* **469**, 189 (2011).
- [13] N. C. Plumb, M. Salluzzo, E. Razzoli, M. Månsson, M. Falub, J. Krempasky, C. E. Matt, J. Chang, M. Schulte, J. Braun, H. Ebert, J. Minár, B. Delley, K.-J. Zhou, T. Schmitt, M. Shi, J. Mesot, L. Patthey, and M. Radović, *ArXiv e-prints* (2013), arXiv:1302.0708 [cond-mat.mtrl-sci].
- [14] M. Kobayashi, I. Muneta, T. Schmitt, L. Patthey, S. Ohya, M. Tanaka, M. Oshima, and V. N. Strocov, *Appl. Phys. Lett.* **101**, 242103 (2012).
- [15] G. Drera, F. Banfi, F. F. Canova, P. Borghetti, L. Sangaletti, F. Bondino, E. Magnano, J. Huijben, M. Huijben, G. Rijnders, and D. H. A. Blank, *Appl. Phys. Lett.* **98**, 052907 (2011).
- [16] A. Koitzsch, J. Ocker, M. Knupfer, M. C. Dekker, K. Dörr, B. Büchner, and P. Hoffmann, *Phys. Rev. B* **84**, 245121 (2011).
- [17] C. Cancellieri, M. L. Reinle-Schmitt, M. Kobayashi, V. N. Strocov, T. Schmitt, P. R. Willmott, S. Gariglio, and J.-M. Triscone, *Phys. Rev. Lett.* **110**, 137601 (2013).
- [18] G. Berner, M. Sing, H. Fujiwara, A. Yasui, Y. Saitoh, A. Yamasaki, Y. Nishitani, A. Sekiyama, N. Pavlenko, T. Kopp, C. Richter, J. Mannhart, S. Suga, and R. Claessen, *Phys. Rev. Lett.* **110**, 247601 (2013).
- [19] A. D. Caviglia, M. Gabay, S. Gariglio, N. Reyren, C. Cancellieri, and J.-M. Triscone, *Phys. Rev. Lett.* **104**, 126803 (2010).
- [20] C. Cancellieri, N. Reyren, S. Gariglio, A. D. Caviglia, A. Fête, and J.-M. Triscone, *Europhys. Lett.* **91**, 17004 (2010).
- [21] A. Filippetti, C. D. Pemmaraju, S. Sanvito, P. Delugas, D. Puggioni, and V. Fiorentini, *Phys. Rev. B* **84**, 195127 (2011).
- [22] V. N. Strocov, T. Schmitt, U. Flechsig, T. Schmidt, A. Imhof, Q. Chen, J. Raabe, R. Betemps, D. Zimoch, J. Krempasky, X. Wang, M. Grioni, A. Piazzalunga, and L. Patthey, *J. Synch. Rad.* **17**, 631 (2010).

- [23] M. L. Reinle-Schmitt, C. Cancellieri, D. Li, D. Fontaine, M. Medarde, E. Pomjakushina, C. W. Schneider, S. Gariglio, P. Ghosez, J.-M. Triscone, and P. R. Willmott, *Nat. Comm.* **3**, 932 (2012).
- [24] N. C. Plumb, M. Kobayashi, M. Salluzzo, E. Razzoli, C. Matt, K.-J. Zhou, C. Monney, T. Schmitt, M. Shi, J. Mesot, L. Patthey, and M. Radović, *ArXiv e-prints* (2013), arXiv:1304.5948 [cond-mat.mtrl-sci].
- [25] Y. Aiura, I. Hase, H. Bando, T. Yasue, T. Saitoh, and D. Dessau, *Surface Science* **515**, 61 (2002).